Medium depth influences O_2 availability and metabolism in cultured RPE cells

Daniel T. Hass[1&], Qitao Zhang[2&], Gillian Autterson[2], Richard Bryan[3], James B. Hurley[1], Jason ML. Miller[2,4]**

[1] Department of Biochemistry, The University of Washington, Seattle WA
[2] Kellogg Eye Center, University of Michigan, Ann Arbor MI
[3] Lucid Scientific, Atlanta GA
[4] Cellular and Molecular Biology Program, University of Michigan, Ann Arbor MI

[&]These authors contributed equally to this manuscript
**Corresponding Author: miljason@umich.edu

Structured Abstract:

Purpose: RPE oxidative metabolism is critical for normal retinal function and is often studied in cell culture systems. Here, we show that conventional culture media volumes dramatically impact O_2 availability, limiting oxidative metabolism. We suggest optimal conditions to ensure cultured RPE is in a normoxic environment permissive to oxidative metabolism.

Methods: We altered the availability of O_2 to human primary RPE cultures directly via a hypoxia chamber or indirectly via the amount of medium over cells. We measured oxygen consumption rates (OCR), glucose consumption, lactate production, $^{13}C_6$-glucose flux, hypoxia inducible factor (HIF-1α) stability, intracellular lipid droplets after a lipid challenge, trans-epithelial electrical resistance, cell morphology, and pigmentation.

Results: Medium volumes commonly employed during RPE culture limit diffusion of O_2 to cells, triggering hypoxia, activating HIF-1α, limiting OCR, and dramatically altering cell metabolism, with only minor effects on typical markers of RPE health. Media volume effects on O_2 availability decrease acetyl-CoA utilization, increase glycolysis, and alter the size and number of intracellular lipid droplets under lipid-rich conditions.

Conclusions: Despite having little impact on visible and typical markers of RPE culture health, media volume dramatically affects RPE physiology “under the hood”. As RPE-centric diseases like age-related macular degeneration (AMD) involve oxidative metabolism, RPE cultures need to be optimized to study such diseases. We provide guidelines for optimal RPE culture volumes that balance ample nutrient availability from larger media volumes with adequate O_2 availability seen with smaller media volumes.

Keywords: retinal pigment epithelium, oxygen, metabolism, isotopic labeling, glucose, lactate, ketone bodies, β-hydroxybutyrate, hypoxia, mitochondria, lipid droplets

Abbreviations:

O2	molecular oxygen
OCR	oxygen consumption rate
RPE	retinal pigment epithelium
hfRPE	human fetal retinal pigment epithelium
LD	Lipid droplet

1. Introduction

Cells use energy released by oxidation of fuels to drive ATP synthesis (1). In the terminal step of the mitochondrial electron transport chain, cytochrome C oxidase reduces O_2 to H_2O. Without O_2, oxidation of metabolic intermediates upstream of cytochrome C oxidase is limited. Accumulation of reduced redox coenzymes under hypoxia leads to a metabolic shift towards glycolysis and lactate production, which generates energy less efficiently. To ensure an adequate O_2 supply for mitochondria, nearly all animals have evolved circulatory and respiratory systems.

In the vertebrate eye, the retinal pigment epithelium (RPE) is a cell monolayer that supports photoreceptor health (2, 3, 4). The RPE is wedged between photoreceptors on its apical surface and a high-flow, fenestrated capillary bed called the choriocapillaris on its basolateral surface. The RPE is the primary site of degeneration in common blinding eye diseases, including Stargardt's disease and age-related macular degeneration (AMD). Numerous lines of evidence support the importance of mitochondrial metabolism in RPE homeostasis: (i) the RPE is among the first tissues in the body affected in inherited mitochondrial disorders (5, 6), (ii) mouse models with defects in RPE mitochondrial function result in RPE phenotypic changes that induce overlying photoreceptor degeneration (7), and (iii) RPE degeneration in AMD is marked by significant mitochondrial structural abnormalities (8, 9). The RPE lives in a synergistic metabolic relationship with overlying photoreceptors, wherein photoreceptors produce lactate and succinate that the RPE consumes (10, 11). RPE mitochondria also consume lipids, which may be derived from phagocytosed photoreceptor outer segments or uptake of lipoprotein particles (12, 13, 14).

Culture of human primary and induced pluripotent stem cell (iPSC)-derived RPE is used widely to model RPE-based retinal degenerations (15, 16, 17, 18, 19, 20, 21). An important assumption in those studies is that atmospheric O_2 concentrations do not limit mitochondrial activity. Estimates *in vivo* suggest that the fractional O_2 availability at the RPE is ~4-9% (extrapolated from (22)), whereas fractional atmospheric O_2 is 21%, suggesting RPE *in vitro* could be in a hyperoxic environment. However, O_2 dissolved in media and consumed by cultures must be replaced by diffusion from air above the medium. *In vivo*, the circulatory system delivers O_2 continuously to within microns of a cellular target. However, *in vitro*, O_2 must diffuse across ~3-25 mm of media to its target, several orders of magnitude greater than diffusion distances *in vivo*. In accordance with Fick's laws, O_2 flux through medium is constrained by the distance over which it must diffuse. If cellular O_2 consumption exceeds O_2 diffusion through culture medium, cells will deplete the medium of O_2 and lose the ability to oxidize fuels (23).

Herein, we test the idea that O_2 consumption by RPE is often greater than diffusion of O_2 into the medium. We use multiple methods to show that widely used media volumes limit O_2 availability in RPE cultures, stabilizing the intracellular hypoxia sensor HIF-1α,

increasing glycolysis, impairing mitochondrial metabolism, and altering intracellular lipid storage. While media volume can dramatically impact RPE metabolism, effects on markers of RPE health are subtle and only apparent after prolonged exposure to higher media volumes. Lower media volumes restore O_2 availability and mitochondrial metabolism but also allow for faster nutrient depletion. Thus, ideal culture conditions for studying RPE function require careful titration of media volume and media change frequency. We provide guidelines for how to optimize media volumes and media change frequencies to preserve mitochondrial metabolism during RPE culture.

2. Materials and Methods

Cell Culture and Trans-Epithelial Electrical Resistance (TEER)

Primary human fetal RPE cultures (hfRPE) were grown and trans-epithelial electrical resistance (TEER) measured according to our detailed protocol outlined earlier (24, 25). All cultures demonstrated robust pigmentation, cobblestone morphology, and TEER of at least 500 Ω*cm^2. All cells for metabolism analysis were passage 1, grown on porous 24-well inserts (Transwells; Corning; product 3470; cell growth area of 0.33 cm^2) for at least 5 weeks before experimentation. Cells for Resipher experiments were grown on tissue-culture treated plastic in 96-well plates (Falcon; Corning; product 353072; cell growth area of 0.32 cm^2) for at least 6 weeks prior to experimentation. Media compositions are based on standard RPE culture media (24, 25, 26, 27), with slight variations for each experiment, as outlined in Supplemental Table 1.

Conjugation of Fatty Acids (FA) to Bovine Serum Albumin

Sodium palmitate (Sigma; product P9767) or sodium oleate (Sigma; product O7501) (FA) was solubilized at 70°C in 150 mM NaCl to create a 12.5 mM solution. The hot 12.5 mM FA solution was transferred to 1.7 mM FA-free BSA (MP Biomedical; product MP219989910) solubilized in glucose-free α-MEM (Supplementary Table 1) at a ratio of 0.8:1 and stirred at 37° C for 1 hour. The molar concentration of the conjugated FA-BSA solution was then adjusted by addition of 150 mM NaCl for a final concentration of 5 mM FA:0.85 mM BSA (6:1 molar ratio). Protocol was adapted from Seahorse Bioscience's "Preparation of Bovine Serum Albumin (BSA)-Conjugated Palmitate."

HIF-1α Staining and Hypoxia Chambers

hfRPE on Transwells were placed in the incubator with either atmospheric O_2 concentrations or in a hypoxia chamber (Billups-Rothenberg, Inc.; product MIC-101) in which O_2 concentration was titrated to 8% utilizing a 1% O_2 / 5% CO_2 / 94% N_2 gas mixture and an O_2 sensor (Sensit P100 Personal Gas Leak Monitor) placed within the hypoxia chamber. After 24 hours of exposure, cells were lysed with 40 µL of 1.2X western blot SDS sample buffer. 100 µM of the prolyl hydroxylase inhibitor DMOG and 10 µM of the protease/phosphatase inhibitor MG-132 (Cell signaling; product 5872S) were used to prevent degradation of HIF. HIF-1α levels were determined in 25 µg lysate

by standard SDS-PAGE and western blot techniques, utilizing a rabbit anti-HIF-1α antibody (Cell signaling; product 36169, 1:1000), a mouse monoclonal anti-GAPDH antibody (EnCor product MCA-1D4), and HRP-linked secondary antibodies (Goat anti-mouse HRP, Jackson Immuno, #115-035-062; Donkey anti-rabbit HRP, #711-035-152, Jackson Immuno).

Lipid Loading and Lipid Droplet Staining

hfRPE on Transwells were loaded with 300 µM BSA-conjugated palmitate in serum-free media (Supplemental Table 1). Cells were incubated at 37℃ for 18 hours and fixed with 4% paraformaldehyde / 4% sucrose solution for 15 minutes. After fixation, photochemical bleaching of the samples was performed. First, 150 µL of freshly made bleaching solution (50 µL deionized formamide, 50 µL of 3M sodium chloride/0.3M sodium citrate, 800 µL water, 163.4 µL 30% hydrogen peroxide) was added to the apical chamber of each Transwell. Next, the liquid light guide of an X-Cite 120Q microscopy system was centered 14 cm over the plate, held in place by a retort stand with utility clamp. After 2 minutes, Transwells were picked up and tapped gently to dislodge bubbles that form on the membrane surface. This step was repeated again at 5-7 minutes. Total bleach time was 15-20 minutes, but should be verified by the degree of pigment visible on the Transwell membrane. Post-bleaching, Transwells were washed 5-8 times with 1x PBS to remove all bubbles. Cells were then quenched with a solution of 50 mM ammonium chloride in PBS for 10 minutes, permeabilized with 0.01% digitonin in PBS for 30 minutes at room temperature (RT), blocked with 3% bovine serum albumin (BSA) in PBS for 20 minutes, and incubated in primary antibody solution (anti-ADRP (perilipin-2), clone AP125 (Progen 610102), 1:10 dilution in 1% BSA in PBS) for 1 hour at RT or overnight at 4° C Secondary antibody incubations and mounting were done in standard fashion, but avoiding all exposure to detergents. Hoechst-34580 (Sigma 63493, 1:500 dilution) was included in the secondary antibody incubation for 1 hour at RT.

Microscopy

Z-stack images were obtained using the Leica STELLARIS 8 FALCON Confocal Microscope and image analysis was performed with Aivia 11 (Leica). To quantify LDs, a pixel classifier and meshes recipe was applied.

Resipher

Resipher (Lucid Scientific, Atlanta, GA, USA) is an instrument that measures oxygen consumption rates (OCR) in standard multiwell culture plates. The device operates by measuring O_2 concentrations across a range of heights in the media above the cell monolayer. These measurements correspond to the O_2 gradient that forms in static media as oxygen diffuses through it. Using these gradient measurements, O_2 flux through the media is calculated using Fick's laws. An introduction to these laws and how they are used is available in the supplementary discussion.

Defined volumes of media were placed over cells and OCR was continuously monitored for up to 5 days without media change. Due to known uneven evaporative effects, wells on the edge of the plate were excluded from analysis. Each volume was tested in at least 6 replicate wells. All wells were confluent with a similar size and number of cells (**Supplemental Figure 1**).

Glucose Concentration Assay

We measured media glucose with an enzymatic assay wherein glucose phosphorylation and oxidation is coupled to $NADP^+$ reduction (28). NADPH absorbs light at 340 nm. We incubated 5 µL culture medium samples and 5 µL of 0-10 mM standards in the following assay buffer: 50 mM Tris, 1 mM $MgCl_2$, 500 µM $NADP^+$, 500 µM ATP, 0.2 U/mL Hexokinase, 0.08 U/mL glucose-6-phosphate dehydrogenase, pH 8.1. Using a BioTek Synergy 4 plate reader, we measured A_{340} over time at 37° C until it reached steady state. We used a linear fit of the standard curve to determine glucose concentrations. We determined glucose amount by multiplying concentrations with apical or basal medium volumes. A complete protocol for the glucose assay, including product numbers, is available at dx.doi.org/10.17504/protocols.io.dm6gpj5jdgzp/v1.

Lactate Concentration Assay

We measured media lactate with an enzymatic assay where lactate dehydrogenase converts lactate and NAD^+ to pyruvate and NADH (28). Pyruvate is consumed by the assay buffer, drawing the reaction to completion. NADH absorbs light at 340 nm. We incubated 5 µL culture medium samples and 5 µL of 0-20 mM standards in the following assay buffer: 300 mM glycine, 166 mM hydrazine, 2.5 mM NAD^+, 8 U/mL lactate dehydrogenase. We determined A_{340} at 37° C with a Bio-Tek Synergy 4 plate-reader. Steady-state A_{340} values from standards were used to determine media [lactate]. A complete protocol for the lactate assay, including product numbers, is available at dx.doi.org/10.17504/protocols.io.6qpvr4733gmk/v1.

Metabolite Extraction and Derivatization

Metabolites were extracted in 80% MeOH, 20% H_2O supplemented with 10 µM methylsuccinate (Sigma; product M81209) as an internal standard. The extraction buffer was equilibrated on dry ice, and 150 µL was added to 2 µL of each medium sample. Samples were incubated on dry ice for 45 minutes to precipitate protein. Proteins were pelleted at 17,000 x g for 30 minutes at 4° C. The supernatant containing metabolites was lyophilized and stored at -80° C until derivatization.

Lyophilized samples were derivatized with 10 µL of 20 mg/mL methoxyamine HCl (Sigma; product 226904) dissolved in pyridine (Sigma; product 270970) and incubated at 37° C for 90 minutes. Samples were further derivatized with 10 µL tert-butyldimethylsilyl-N-methyltrifluoroacetamide (Sigma; product 394882) and incubated at 70° C for 60 minutes.

Gas Chromatography-Mass Spectrometry

Metabolites were analyzed on an Agilent 7890/5975C GC-MS using methods described extensively in previous work (29). Briefly, 1 µL of derivatized sample is injected and delivered to an Agilent HP-5MS column by helium gas (1 mL/min). The temperature gradient starts at 100° C for 4 minutes and increases 5° C/min to 300° C, where it is held for 5 minutes. We used select ion monitoring (SIM) to record ions (m/z: ~50–600) in expected retention time windows. Peaks were integrated in MSD ChemStation (Agilent). We corrected for natural isotope abundance using IsoCor (30). Corrected metabolite signals were converted to molar amounts by comparing metabolite peak abundances in samples with those in a standard mix. Multiple concentrations of this mix were extracted, derivatized, and run alongside samples in each experiment.

Statistical Analysis

All figures representing data in this manuscript represent either individual data points or the arithmetic mean, ± standard error. Western blot data was analyzed with one-way ANOVA or a student's t-test. The significance threshold for statistical tests was set as: *$p \leq 0.05$, ***$p \leq 0.001$. All statistics were calculated using Prism v9.5.0 (GraphPad Software, LLC)

3. Results

3.1. The volume of cell culture media determines the balance between hypoxic conditions and nutrient availability, with only subtle effects on markers of RPE health

Primary human fetal RPE (hfRPE) cultures were grown on Transwell filters in 24-well plates to best mimic cellular polarity and access to nutrients *in vivo*. We have previously established these cultures as highly polarized and differentiated, with high TEER, expression of RPE-specific expression markers, high pigmentation, and capacity for photoreceptor outer segment (OS) phagocytosis (24). The apical side of the filter faces the air-medium interface, and the basal surface faces the bottom of the culture plate.

O_2 can reach cells through either chamber (**Figure 1A**) but the apical chamber media directly touches cells without an intervening membrane and unrestricted access to the atmosphere, so we chose to alter apical media volumes to understand the effect of media volume on O_2 availability at the cell monolayer. We hypothesized that O_2 availability and, therefore, O_2 consumption rate (OCR) are limited by medium depth under standard culture conditions, where apical medium volume usually varies between 100 µL and 200 µL. To test this hypothesis, we grew hfRPE on 96-well plastic plates, which have the same surface area as a 24-well Transwell. We used the Resipher system to measure OCR when the well was filled with 65, 95, 125, or 200 µL of media. The Resipher instrument determines OCR based on the vertical [O_2]-gradient that develops within the medium in the well. OCR is lowest at 200 µL (<100 fmol/mm^2/second) but increases at lower apical medium volumes (**Figure 1B,C**), showing that OCR is indeed limited in a medium volume-dependent manner. Steady-

state OCR is nearly identical at 65 and 95 µL medium at 140-160 fmol/mm^2/second, suggesting that at volumes just under 100 µL, [O_2] no longer limits oxidative phosphorylation (**Figure 1B,C**). Given a cell culture surface area of 0.33 cm^2, this corresponds to a media volume to surface area ratio of 300 µL/cm2. These OCR values, stable for almost a day, represent how the cultures initially respond to O_2 limitation. With additional time, cultures with larger volumes further adapt OCR to limited O_2 availability.

Our OCR data imply that hfRPE could be hypoxic when cultured at >300 µL/cm^2. To confirm that our cells under higher media volumes were sensing hypoxia, we measured cellular levels of the hypoxia responsive transcription factor, HIF-1α. HIF-1α is degraded when hydroxylated, and the ability of cells to hydroxylate HIF-1α depends on the availability of O_2 (31). Thus, low O_2 concentrations increase HIF-1α levels. We treated hfRPE on Transwells at 8% atmospheric or 21% atmospheric O_2 for 24 hours, and at each atmospheric O2 concentration also modulated apical medium volume, while keeping basolateral media volume consistent at 400 µL. Western blot of hfRPE lysate revealed a clear effect of both medium depth and of atmospheric [O_2] on HIF-1α, supporting the conclusion that increasing medium volumes can lead to hypoxia in culture (**Figure 1D).** Notably, while 8% O_2 is considered physioxic *in vivo*, 8% atmospheric O_2 increases HIF-1α levels *in vitro*. Even under the lowest culture volume, 65 µL, HIF-1α was significantly more stabilized in the 8% O_2 conditions than the 21% O_2 conditions (**Figure 1D;** bottom right). This reaffirms that high diffusion distance *in vitro* limits O_2 access to cells and complicates comparisons of O_2 concentrations *in vivo* with O2 concentrations *in vitro*.

Unfortunately, while lower media volumes improve O_2 availability, they also limit nutrient supply. The typical interval between medium changes in RPE cultures is 48-72 hours. To measure the effects of media volume on substrate depletion rates, we supplied 65, 95, 125, or 200 µL medium to hfRPE and measured OCR up to 120 hours. We hypothesized and confirmed that when all mitochondrial substrates have been consumed, OCR will drop. With 65 µL, the time to a 50% drop from steady-state OCR is 76.7 ± 1.3 (mean ± SEM) hours after a medium change. With 95 µL, OCR dropped to 50% by 109 ± 4.2 hours after a medium change. At greater medium depths, OCR persisted at steady-state levels past 120 hours. Thus, at media volumes just under a ratio of 300 µL/cm^2, RPE grows without O_2 limitation and requires twice weekly media changes to prevent a decrease in OCR that would indicate insufficient fuel availability (**Figure 1E**).

To determine the effects of media volume on typical markers of RPE health, we examined tight-junction integrity, morphology, and pigmentation (32). We previously established trans-epithelial electrical resistance (TEER) as a sensitive marker for subtle cell death (33). hfRPE cultures supplied with 100 µL or 200 µL of media for up to three weeks had no differences in cell morphology or pigmentation (**Supplemental Figure 2A**), but subtle differences in TEER that were present only after exposure for 3 weeks and not 1 week (**Supplemental Figure 2B**). These results suggest extremely slow

cumulative dysfunction to cultures over time which are not apparent by simple visual inspection.

3.2. Limiting O2-dependent metabolism accelerates glycolysis, depleting glucose faster and causing an accumulation of lactate

When O_2 -availability limits mitochondrial metabolism, cells can process glucose by reducing pyruvate into lactate. This mode of glucose utilization produces ATP at only 1/16th the efficiency as complete oxidation of glucose to CO_2, so more glucose is consumed to support the same energetic needs.

As a proof of this concept in RPE, we examined the effects of limiting O_2 availability on glucose consumption and lactate production in our hfRPE cultures. We cultured cells on Transwells with 100 µL apical medium and 200 µL basolateral media over 24 hours, where the cells were equilibrated with 21% O_2 in air. Next, we incubated the same cells in the same media volume but set O_2 at 8% in air. We measured total glucose and total lactate content in culture medium before it was exposed to cells and after 24 hours via an enzymatic assay. 8% O_2 was sufficient to increase glucose utilization (**Figure 2A**) and lactate production (**Figure 2B**) such that almost all glucose provided to the 8% O_2 RPE cells was consumed within 24 hours.

To determine whether higher medium volumes had the same effect on glucose consumption and lactate production as 8% O_2, we cultured hfRPE in ambient oxygen (21% O_2) for 22 hours in 65, 125, or 200 µL of apical media and 400 uL of media basolaterally. We replaced normal unlabeled glucose (5 mM) with the same concentration of $^{13}C_6$-glucose and supplemented medium with 150 µM palmitate-BSA and 150 µM oleate-BSA to provide substrates used by mitochondria. We probed metabolite release into the apical and basal chambers through a combination of mass spectrometry and enzymatic assays. The metabolite amounts represent the sum of apical and basal metabolite content (**Figures 2, 3**).

RPE glucose consumption (from 4-22 hours) increases with greater apical medium depth (**Figure 2C-D**), and lactate production follows the same trend (**Figure 2E-F**). When measuring glucose and lactate levels, we noticed that for the first 4 hours after a medium change, glycolytic flux was insensitive to apical medium depth, and differences between conditions only appeared between 4 and 22 hours in culture. We hypothesized that O_2 gradients leading to cellular hypoxia take time to develop, such that glucose and lactate levels in the different medium depths would only differ after steady-state establishment of O_2 gradients. Indeed, when we measured the O_2 concentration 1 mm above cells over time using the Resipher device, we found limits in O_2 availability developed only after several hours (**Figure 2G**).

As pyruvate and other fuels were present in the medium, we entertained the possibility that these metabolites could be sources of lactate independent of glucose. To trace the fate of glucose under different media volumes, we quantified $^{13}C_6$-glucose-derived glycolytic products (which are m+3 labeled). After the O_2 gradient is established,

glucose-derived lactate (**Figure 2H**) and pyruvate (**Figure 2I**) (each m+3) both increase in an apical volume-dependent manner. This directly indicates an acceleration in the rate of glycolysis with greater medium depth.

3.3. Acetyl-CoA utilization increases with decreasing medium depth

With decreasing apical medium volumes, more O_2 is delivered to mitochondria, which should enable mitochondrial TCA cycle activity and β-oxidation to proceed. In the first step of mitochondrial energy metabolism of glucose, pyruvate is decarboxylated to acetyl-CoA, which can enter the TCA cycle. $^{13}C_6$-glucose is used to synthesize m+2 acetyl-CoA, which is then used to make m+2 citrate and m+2 labeled downstream intermediates. Many intermediates produced from acetyl-CoA are exported from mitochondria and cells, so sampling media above cells provides a noninvasive way to assess metabolism of ^{13}C tracers.

Growing hfRPE on Transwells under conditions identical to those in Figure 2, we found a clear relationship between media depth and labeled intermediates secreted into the media. As apical medium depth decreases, more m+2 citrate is made (**Figure 3A**) and a greater proportion of citrate is ^{13}C-labeled (**Figure 3B**). The trend exists for downstream TCA cycle and anapleurotic intermediates such as malate (**Figure 3C-D**) and glutamate (**Figure 3E-F**).

β-hydroxybutyrate (β-HB) is a ketone body made using carbons from two acetyl-CoA molecules, and the RPE's capacity for ketogenesis is well established (13, 15). While glucose can fuel β-HB production, ketogenesis is often considered primarily to be a product of fatty acid metabolism (34, 35) that occurs in the mitochondria. Compared with exported TCA cycle intermediates, most of the β-HB produced by hfRPE over 22 hours is unlabeled (**Figure 3G-H**), suggesting that it is not derived from $^{13}C_6$-glucose but instead from unlabeled fatty acids that we provided in the medium. As with TCA cycle intermediates, production of fatty acid-derived m+0 β-HB also increased at the lowest medium volume (**Figure 3G**), suggesting fatty acid metabolism in RPE culture may be limited at higher medium volumes.

3.4. Mass action is not the sole driver of differences in metabolite release rates between different volume conditions

The law of mass action states that reaction rate is proportional to concentration of products and reactants. Applied to metabolite export into medium, the law suggests that the ratio of the metabolite's intracellular vs. extracellular concentration will dictate the rate of export. Higher medium volumes dilute metabolites more, and thus support faster export rates. Therefore medium depth can affect cellular metabolism not only by altering cellular O_2 and nutrient availability, but also through mass action. We tested whether this confounding variable could drive metabolic effects of media volume unrelated to O_2 supply.

While apical volumes in our experimental set-up differ, basal volumes are constant. Thus, metabolite efflux to the basal side should exclusively reflect O_2-dependent differences in hfRPE metabolism. When labeling of lactate, pyruvate, and citrate from $^{13}C_6$-glucose is measured separately in apical and basal chambers, there is a clear effect of volume on the flux of m+3 lactate (**Figure 4A**), m+3 pyruvate (**Figure 4B**), and m+2 citrate (**Figure 4C**) in both chambers. Thus, while mass action may play a general role in metabolite release, medium depth-dependent differences in O2 drive differential metabolite release to the basal chamber.

3.5. Media volume affects lipid droplet dynamics after RPE lipid challenge

The RPE is a prolific consumer of lipids (36). A previous study has shown that the RPE forms temporary lipid droplets (LDs) in response to such lipid challenges (37), and the ability of other cell types to mitochondrially metabolize fatty acids released from lipid droplets partly controls the size and persistence of LDs (38). As fatty acid β-oxidation is O_2-dependent, we hypothesized that higher media volumes would inhibit β-oxidation, resulting in altered LD dynamics. To test this hypothesis, we fed hfRPE serum-free media supplemented with 300 µM BSA-conjugated palmitate for 18 hours, comparing LD formation with an apical volume of 65 µL vs. 200 µL (with a constant basal volume of 400 µL and 21% atmospheric O2). As a control for limited O_2 availability but equal absolute amounts of palmitate, we also provided cells with 65 µL of medium under 1% atmospheric O_2. Decreasing O_2 levels via 1% atmospheric O_2 or higher media volumes had a similar effect on increasing LD amount and size (**Figure 5A-C**). Interestingly, larger LD were also more likely to be localized basolaterally (**Figure 5D**). Thus, studies exploring the role of lipid metabolism and LDs in the RPE need to be particularly cognizant of media volume effects.

4. Discussion

Degeneration of the RPE underlies some of the most common causes of vision loss. As the RPE is heavily reliant on mitochondrial metabolism and mitochondrial defects have been demonstrated in myriad RPE-centric diseases, there has been an explosion of disease-oriented research on RPE oxidative metabolism (3), including in RPE cultures. While primary and iPSC-derived RPE cultures models have shown great promise in recapitulating characteristics of RPE in health and disease, we show that media volumes commonly employed for RPE culture can profoundly limit O_2 availability. This impacts everything from mitochondrial metabolism to activation of hypoxia-responsive transcription factors to lipid droplet dynamics.

In this paper, we show that the higher end of media depths commonly utilized in RPE culture induce hypoxia. Cellular O_2 availability depends on both media depth, which is determined by the ratio of media volume to surface area for cell culture, and the OCR rate for the type of cells being studied. If the cell demonstrates high mitochondrial metabolism, OCR will be higher and O_2 will be depleted faster, necessitating a lower media depth to ensure adequate O_2 supply. In this study, using mature, polarized, confluent primary human RPE cultures, RPE OCR necessitates a volume/surface area

ratio of 300 µL/cm^2 or lower to avoid hypoxia at the cell monolayer. Media volume to surface area ratios lower than 300 µL/ cm^2 would improve O_2 availability further, but are not necessary because they do not further increase OCR and could restrict nutrient availability. Indeed, at a volume/surface area ratio of approximately 200 µL/cm^2 (65 µL in 24-well Transwell) , nutrient depletion *begins* to affect mitochondrial metabolism after approximately 50-55 hours, whereas at a ratio of approximately 300 µL/cm^2 (95 µL in 24-well Transwell), nutrient depletion doesn't *begin* to affect mitochondrial metabolism until approximately 80-85 hours (**Figure 1B**). Since most labs change cell culture media between 2-3 times per week, a volume/surface area ratio of approximately 300 µL/cm^2 represents the ideal balance between O_2 and nutrient availability for hfRPE.

Factors other than media depth and OCR also influence O_2 availability *in vitro*. These include diffusion of O_2 through the plastic sides and bottom surface of the well, humidity in the incubator, and the atmospheric pressure (e.g. - in labs at elevation) (28). These effects can only partially be controlled, but can be compensated for by altering medium volume. To estimate the consequences of manipulating medium volume and other parameters on cellular O_2 availability, we designed an interactive web notebook, available at: https://observablehq.com/@lucid/oxygen-diffusion-and-flux-in-cell-culture. The assumptions and calculations underpinning the calculator within the notebook are outlined in the Supplementary Discussion.

Our studies show that media volume effects on O_2 availability profoundly influence RPE glycolytic and mitochondrial metabolism. At higher media volumes, higher glucose consumption and lactate production predominate, with diminished incorporation of glucose carbons into TCA cycle intermediates and glutamate. Our data recapitulate similar findings in adipocytes (23).

The RPE is a high-volume consumer of lipids, and the pathogenesis of AMD, an RPE-centric degeneration, is thought to involve RPE lipid handling (39). Thus, there is intense interest in understanding and manipulating RPE β-oxidation for therapeutic purposes. Our media volume data suggests, however, that *in vitro* studies on lipid metabolism in the RPE may be hampered by limited O_2 availability. Numerous studies have established that LDs increase dramatically under hypoxia or conditions that activate the hypoxia-sensing cellular machinery (40, 41). In our cultures, limited O2 availability from higher media volumes altered LD number, size, and polarized intracellular localization after lipid challenge. Interestingly, a prior paper demonstrated that hypoxia is known to specifically stimulate larger LDs (42).

While the effects of media volume on central carbon and lipid metabolism in our culture system was profound, the effects on commonly employed markers for RPE health were much more subtle. There were no effects on RPE morphology or pigmentation, even with prolonged (3 week) exposure to high media volumes. The effects on TEER were subtle. This uncoupling between highly altered cellular metabolism and unaltered RPE function/survival explains why the effects of media volume on RPE cultures have largely been ignored to date. We suggest the RPE may be highly adaptable, capable of

metabolic states *in vitro* that promote survival despite deviating significantly from their *in vivo* metabolic state.

Hypoxia inducible factor (HIF), a hypoxia-responsive transcription factor, plays an important part in RPE pathophysiology, and we found that HIF-1α is stabilized in media volumes commonly employed for RPE culture. Given HIF's documented role in various RPE pathologies (41, 43, 44), investigating normal RPE biology under standard media volume conditions that constitutively activate HIF could be misleading.

In conclusion, media depth is a critical factor in determining O_2 availability in RPE culture, with myriad serious consequences disguised underneath normal-appearing morphology and pigmentation. Unfortunately, medium volume is rarely reported in studies on RPE culture, including by our own prior publications. To ensure more consistency across studies on RPE metabolism and mitochondrial health, we recommend reporting cell culture surface area, confluency, media volume, and time between media change and the end-point of the experiment, at a minimum. For RPE cultures with OCR rates similar to hfRPE, we recommend maintaining cultures at 300 µL of media per cm^2 of surface area, and going no longer than four days between media changes.

Acknowledgements

Figure panel 1A was created with BioRender.com. We thank Dr. Subramaniun Pennathur for helpful comments.

Funding sources

J.M.L.M. is supported by a career development grant by the National Eye Institute (K08EY033420). This work is also supported by the James Grosfeld Initiative for Dry AMD (https://jasonmiller.lab.medicine.umich.edu/links). D.T.H is supported by a Brightfocus Foundation Postdoctoral Fellowship (M2022003F). J.B.H is supported by NEI RO1EY06641, RO1EY017863 and R21032597.

Figure captions

Figure 1. Medium volume limits cellular O_2 uptake by increasing O_2 diffusion distance. (A) Schematic showing the path O_2 must take to get from air, through liquid barriers (culture medium), and to cells at varying apical volumes and constant basal volume. (**B**) OCR over time for wells at different medium depths (65, 95, 125, 200 µL; n=6 wells/group). (**C**) Average initial steady-state OCR at each medium depth. (**D**) [O_2]-dependent or medium volume-dependent changes in HIF-1α, as assessed by Western blot (normalized to GAPDH) (n=3). (**E**) Medium volume also affects mitochondrial fuel availability. As these fuels are depleted, OCR drops. Plotted is the time (in hours) after media change until OCR drops to 50% of its previous steady-state (n=6). *$p \leq 0.05$, student's T-test.

Figure 2. Glycolysis is accelerated by increasing medium depth. (A) Medium glucose and **(B)** medium lactate amounts after 24 hours of culture in medium without cells, medium with cells at 21% atmospheric O_2, or cells at 8% atmospheric O_2. Decreased O_2 levels increase glucose utilization and lactate production. **(C-D)** Increasing medium volume also limits cellular O_2 availability, increasing glucose consumption and **(E-F)** lactate production. **(G)** Limited cellular O_2 availability develops only after several hours in culture as steady-state O_2 diffusion gradients develop. This explains why medium volume effects on glucose and lactate (C-F) develop only after 4 hours. **(H-I)** Decreased glucose levels and increased lactate levels are a direct consequence of glucose consumption, as assessed by $^{13}C_6$-glucose tracing to m+3 lactate **(H)** and m+3 pyruvate **(I)** (n=5-6).

Figure 3. Mitochondrially-dependent acetyl-CoA utilization increases with decreasing medium depth. We traced the fate of $^{13}C_6$-glucose into mitochondrially-dependent intermediates, measuring the rate of appearance of m+2 labeled intermediates in the apical media from 4-22 hours after media change (**A,C,E)**, as well as the fraction of each intermediate in the apical vs. basolateral media that picked up a ^{13}C label at 22 hours **(B,D,F)**. The apical media secretion rate of citrate **(A)**, malate **(C)**, and **(E)** glutamate derived from glucose (m+2) decreases with higher media volumes. In addition, the fraction of total **(B)** citrate, **(D)** malate, and **(F)** glutamate with a ^{13}C label decreases at higher media volumes. These results confirm that limited O_2 diffusion to cells prevents ongoing mitochondrial activity. **(G)** The total and unlabeled (m+0) β-HB in the apical media were almost identical, suggesting that glucose does not contribute to ketogenesis. β-HB present in apical media likely derives from unlabeled fatty acids added to the cultures. Similar to other mitochondrially-dependent intermediates, β-HB production was highest at the lowest media volume where O_2 availability is not limiting. **(H)** Fractional labeling of β-HB from $^{13}C_6$-glucose confirms almost no production of β-HB from glucose (n=5-6).

Figure 4. Volume effects on metabolite release rates depend largely on O_2 availability. Given different apical volumes, differences in metabolite release rates into the medium could be caused by differences in O_2 availability or simply mass action effects. While apical media volumes differ, basal media volumes are constant across all conditions. Thus, release of metabolites into the basolateral media will be unaffected by mass action, and any apical media volume effects on basal metabolite release must be due to differences in O_2 availability between the conditions. **(A)** The release rate of m+3 lactate derived from $^{13}C_6$-glucose into the apical (black dots) or basal (pink dots) chambers from 4-22 hours are similarly affected by apical media volume, confirming O_2 availability is the dominant factor affecting release. Similar analysis for **(B)** pyruvate and **(C)** citrate.

Figure 5. Media volume affects RPE lipid droplet size, number, and localization after lipid challenge. In both hypoxic (1% O_2) and high media volume (200 µL) conditions, there is an increase in the **(A)** number of lipid droplets (LD) and **(B)** size of LD formed after 18 hour lipid challenge (300 µM palmitate). n=3-4 randomly selected

images. **(C)** Immunostaining LD (ADRP/perilipin-2, green) and nuclei (Hoechst 34580, blue) under high volume or 1% O_2 conditions. **(D)** The larger LD that form under high volume or low atmospheric O_2 conditions are predominantly basolateral (red arrowhead), adjacent to nuclei. The smaller LD that form under normoxia are more apically localized (white arrowhead). Scale bar= 10 µM for X-Y and X-Z images.

Supplemental Figure 1. Number of highly differentiated confluent RPE cells is consistent between cell culture wells. Manually counted cell numbers from same size images randomly taken in the center of 8 wells were normalized to the average.

Supplemental Figure 2. Higher media volumes cause mild alterations in typical markers of RPE health. (A) Brightfield images show similar polygonal shape and pigmentation for RPE under 100 µL and 200 µL apical (basal 600 µL) media volume after 3 weeks. Scale bar = 10 µM. **(B)** TEER was measured at day 0, 7, and 21 days after culturing in 100 µL or 200 µL apical media (basal 600 µL), with subtle differences emerging only after 3 weeks. ns, not significant, *, $p \leq 0.05$. TEER readings were normalized to starting TEER value on day 0 and 100 µL value. n=6.

References

1. Mitchell P. Coupling of phosphorylation to electron and hydrogen transfer by a chemi-osmotic type of mechanism. Nature. 1961;191:144-8.
2. Swarup A, Samuels IS, Bell BA, Han JYS, Du J, Massenzio E, et al. Modulating GLUT1 expression in retinal pigment epithelium decreases glucose levels in the retina: impact on photoreceptors and Müller glial cells. Am J Physiol Cell Physiol. 2019;316(1):C121-C33.
3. Lakkaraju A, Umapathy A, Tan LX, Daniele L, Philp NJ, Boesze-Battaglia K, et al. The cell biology of the retinal pigment epithelium. Prog Retin Eye Res. 2020:100846.
4. Chowers G, Cohen M, Marks-Ohana D, Stika S, Eijzenberg A, Banin E, et al. Course of Sodium Iodate-Induced Retinal Degeneration in Albino and Pigmented Mice. Invest Ophthalmol Vis Sci. 2017;58(4):2239-49.
5. Latvala T, Mustonen E, Uusitalo R, Majamaa K. Pigmentary retinopathy in patients with the MELAS mutation 3243A-->G in mitochondrial DNA. Graefes Arch Clin Exp Ophthalmol. 2002;240(10):795-801.
6. Tsang SH, Aycinena ARP, Sharma T. Mitochondrial Disorder: Maternally Inherited Diabetes and Deafness. Adv Exp Med Biol. 2018;1085:163-5.
7. Zhao C, Yasumura D, Li X, Matthes M, Lloyd M, Nielsen G, et al. mTOR-mediated dedifferentiation of the retinal pigment epithelium initiates photoreceptor degeneration in mice. J Clin Invest. 2011;121(1):369-83.
8. Ferrington DA, Fisher CR, Kowluru RA. Mitochondrial Defects Drive Degenerative Retinal Diseases. Trends Mol Med. 2020;26(1):105-18.
9. Kaarniranta K, Uusitalo H, Blasiak J, Felszeghy S, Kannan R, Kauppinen A, et al. Mechanisms of mitochondrial dysfunction and their impact on age-related macular degeneration. Prog Retin Eye Res. 2020;79:100858.
10. Kanow MA, Giarmarco MM, Jankowski CS, Tsantilas K, Engel AL, Du J, et al. Biochemical adaptations of the retina and retinal pigment epithelium support a metabolic ecosystem in the vertebrate eye. Elife. 2017;6.

11. Bisbach CM, Hass DT, Robbings BM, Rountree AM, Sadilek M, Sweet IR, et al. Succinate Can Shuttle Reducing Power from the Hypoxic Retina to the O2 Rich Pigment Epithelium. Cell Rep. 2020;31(5):107606.
12. Fisher CR, Ferrington DA. Perspective on AMD Pathobiology: A Bioenergetic Crisis in the RPE. Invest Ophthalmol Vis Sci. 2018;59(4):AMD41-AMD7.
13. Reyes-Reveles J, Dhingra A, Alexander D, Bragin A, Philp NJ, Boesze-Battaglia K. Phagocytosis-dependent ketogenesis in retinal pigment epithelium. J Biol Chem. 2017;292(19):8038-47.
14. Adijanto J, Du J, Moffat C, Seifert EL, Hurle JB, Philp NJ. The retinal pigment epithelium utilizes fatty acids for ketogenesis. J Biol Chem. 2014;289(30):20570-82.
15. Adijanto J, Philp NJ. Cultured primary human fetal retinal pigment epithelium (hfRPE) as a model for evaluating RPE metabolism. Exp Eye Res. 2014;126:77-84.
16. Bharti K, den Hollander AI, Lakkaraju A, Sinha D, Williams DS, Finnemann SC, et al. Cell culture models to study retinal pigment epithelium-related pathogenesis in age-related macular degeneration. Exp Eye Res. 2022;222:109170.
17. Galloway CA, Dalvi S, Hung SSC, MacDonald LA, Latchney LR, Wong RCB, et al. Drusen in patient-derived hiPSC-RPE models of macular dystrophies. Proc Natl Acad Sci U S A. 2017;114(39):E8214-E23.
18. George A, Sharma R, Pfister T, Abu-Asab M, Hotaling N, Bose D, et al. In vitro disease modeling of oculocutaneous albinism type 1 and 2 using human induced pluripotent stem cell-derived retinal pigment epithelium. Stem Cell Reports. 2022;17(1):173-86.
19. Rabin DM, Rabin RL, Blenkinsop TA, Temple S, Stern JH. Chronic oxidative stress upregulates Drusen-related protein expression in adult human RPE stem cell-derived RPE cells: a novel culture model for dry AMD. Aging (Albany NY). 2013;5(1):51-66.
20. Zhang Q, Presswalla F, Calton M, Charniga C, Stern J, Temple S, et al. Highly Differentiated Human Fetal RPE Cultures Are Resistant to the Accumulation and Toxicity of Lipofuscin-Like Material. Invest Ophthalmol Vis Sci. 2019;60(10):3468-79.
21. Zhang Q, Presswalla F, Ali RR, Zacks DN, Thompson DA, Miller JML. Pharmacologic activation of autophagy without direct mTOR inhibition as a therapeutic strategy for treating dry macular degeneration. Aging (Albany NY). 2021;13(8):10866-90.
22. Linsenmeier RA, Zhang HF. Retinal oxygen: from animals to humans. Prog Retin Eye Res. 2017;58:115-51.
23. Tan J, Virtue S, Norris DM, Conway OJ, Yang M, Gribben C, et al. Oxygen is a critical regulator of cellular metabolism and function in cell culture. bioRxiv. 2022:2022.11.29.516437.
24. Zhang Q, Presswalla F, Feathers K, Cao X, Hughes BA, Zacks DN, et al. A platform for assessing outer segment fate in primary human fetal RPE cultures. Exp Eye Res. 2019;178:212-22.
25. Maminishkis A, Chen S, Jalickee S, Banzon T, Shi G, Wang FE, et al. Confluent monolayers of cultured human fetal retinal pigment epithelium exhibit morphology and physiology of native tissue. Invest Ophthalmol Vis Sci. 2006;47(8):3612-24.
26. Fernandes M, McArdle B, Schiff L, Blenkinsop TA. Stem Cell-Derived Retinal Pigment Epithelial Layer Model from Adult Human Globes Donated for Corneal Transplants. Curr Protoc Stem Cell Biol. 2018;45(1):e53.
27. Sharma R, Bose D, Montford J, Ortolan D, Bharti K. Triphasic developmentally guided protocol to generate retinal pigment epithelium from induced pluripotent stem cells. STAR Protoc. 2022;3(3):101582.
28. Seidemann J. Lowry, O. H., und J. V. Passonneau: A flexible system of enzymatic analysis. Academic Press, New York, 1972. 291 S., 32 Abb., 15 Tab., Preis $ 14.00. Starch - Stärke. 1973;25(9):322-.
29. Du J, Rountree A, Cleghorn WM, Contreras L, Lindsay KJ, Sadilek M, et al. Phototransduction Influences Metabolic Flux and Nucleotide Metabolism in Mouse Retina. J Biol Chem. 2016;291(9):4698-710.

30. Millard P, Delépine B, Guionnet M, Heuillet M, Bellvert F, Létisse F. IsoCor: isotope correction for high-resolution MS labeling experiments. Bioinformatics. 2019;35(21):4484-7.
31. Safran M, Kaelin WG. HIF hydroxylation and the mammalian oxygen-sensing pathway. J Clin Invest. 2003;111(6):779-83.
32. Schaub NJ, Hotaling NA, Manescu P, Padi S, Wan Q, Sharma R, et al. Deep learning predicts function of live retinal pigment epithelium from quantitative microscopy. J Clin Invest. 2020;130(2):1010-23.
33. Miller JML, Zhang Q, Johnson MW. Regression of drusen or vitelliform material heralding geographic atrophy: correlation between clinical observations and basic science. Graefes Arch Clin Exp Ophthalmol. 2021;259(7):2051-3.
34. Hui S, Cowan AJ, Zeng X, Yang L, TeSlaa T, Li X, et al. Quantitative Fluxomics of Circulating Metabolites. Cell Metab. 2020;32(4):676-88.e4.
35. Robinson AM, Williamson DH. Physiological roles of ketone bodies as substrates and signals in mammalian tissues. Physiol Rev. 1980;60(1):143-87.
36. Lewandowski D, Sander CL, Tworak A, Gao F, Xu Q, Skowronska-Krawczyk D. Dynamic lipid turnover in photoreceptors and retinal pigment epithelium throughout life. Prog Retin Eye Res. 2022;89:101037.
37. Baker BN, Moriya M, Maude MB, Anderson RE, Williams TP. Oil droplets of the retinal epithelium of the rat. Exp Eye Res. 1986;42(6):547-57.
38. Rambold AS, Cohen S, Lippincott-Schwartz J. Fatty acid trafficking in starved cells: regulation by lipid droplet lipolysis, autophagy, and mitochondrial fusion dynamics. Dev Cell. 2015;32(6):678-92.
39. Jun S, Datta S, Wang L, Pegany R, Cano M, Handa JT. The impact of lipids, lipid oxidation, and inflammation on AMD, and the potential role of miRNAs on lipid metabolism in the RPE. Exp Eye Res. 2019;181:346-55.
40. Boström P, Magnusson B, Svensson PA, Wiklund O, Borén J, Carlsson LM, et al. Hypoxia converts human macrophages into triglyceride-loaded foam cells. Arterioscler Thromb Vasc Biol. 2006;26(8):1871-6.
41. Kurihara T, Westenskow PD, Gantner ML, Usui Y, Schultz A, Bravo S, et al. Hypoxia-induced metabolic stress in retinal pigment epithelial cells is sufficient to induce photoreceptor degeneration. Elife. 2016;5.
42. de la Rosa Rodriguez MA, Kersten S. Regulation of lipid droplet homeostasis by hypoxia inducible lipid droplet associated HILPDA. Biochim Biophys Acta Mol Cell Biol Lipids. 2020;1865(9):158738.
43. Kong Y, Liu PK, Li Y, Nolan ND, Quinn PMJ, Hsu CW, et al. HIF2α activation and mitochondrial deficit due to iron chelation cause retinal atrophy. EMBO Mol Med. 2023;15(2):e16525.
44. Kurihara T, Westenskow PD, Friedlander M. Hypoxia-inducible factor (HIF)/vascular endothelial growth factor (VEGF) signaling in the retina. Adv Exp Med Biol. 2014;801:275-81.

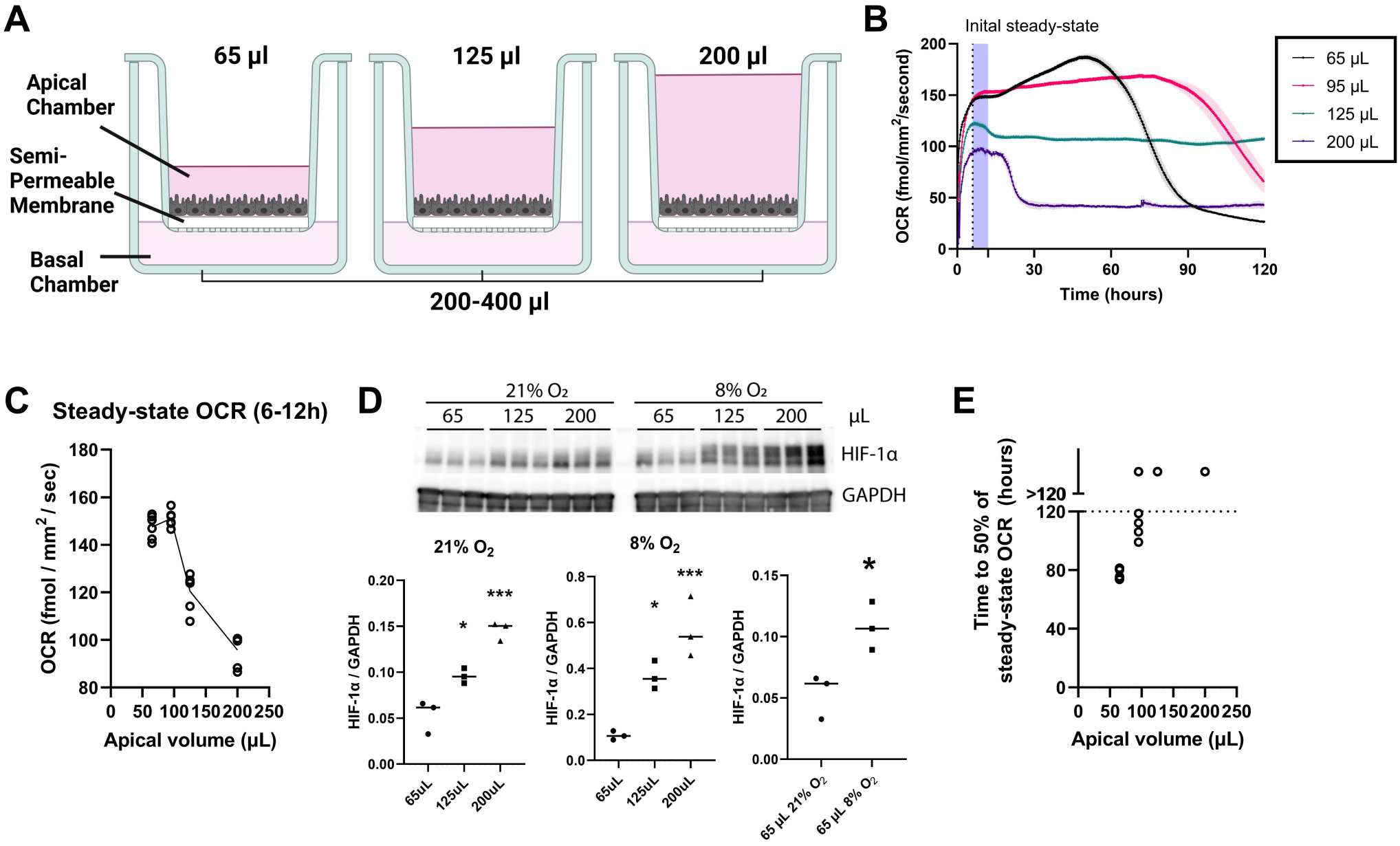
A
65 µl
125 µl
200 µl
Apical Chamber
Semi-Permeable Membrane
Basal Chamber
200-400 µl
B
Inital steady-state
OCR (fmol/mm²/second)
Time (hours)
65 µL
95 µL
125 µL
200 µL
C
Steady-state OCR (6-12h)
OCR (fmol / mm² / sec)
Apical volume (µL)
D
21% O₂
8% O₂
65
125
200
µL
HIF-1α
GAPDH
21% O₂
8% O₂
HIF-1α / GAPDH
65uL
125uL
200uL
65 µL 21% O₂
65 µL 8% O₂
E
Time to 50% of steady-state OCR (hours)
Apical volume (µL)

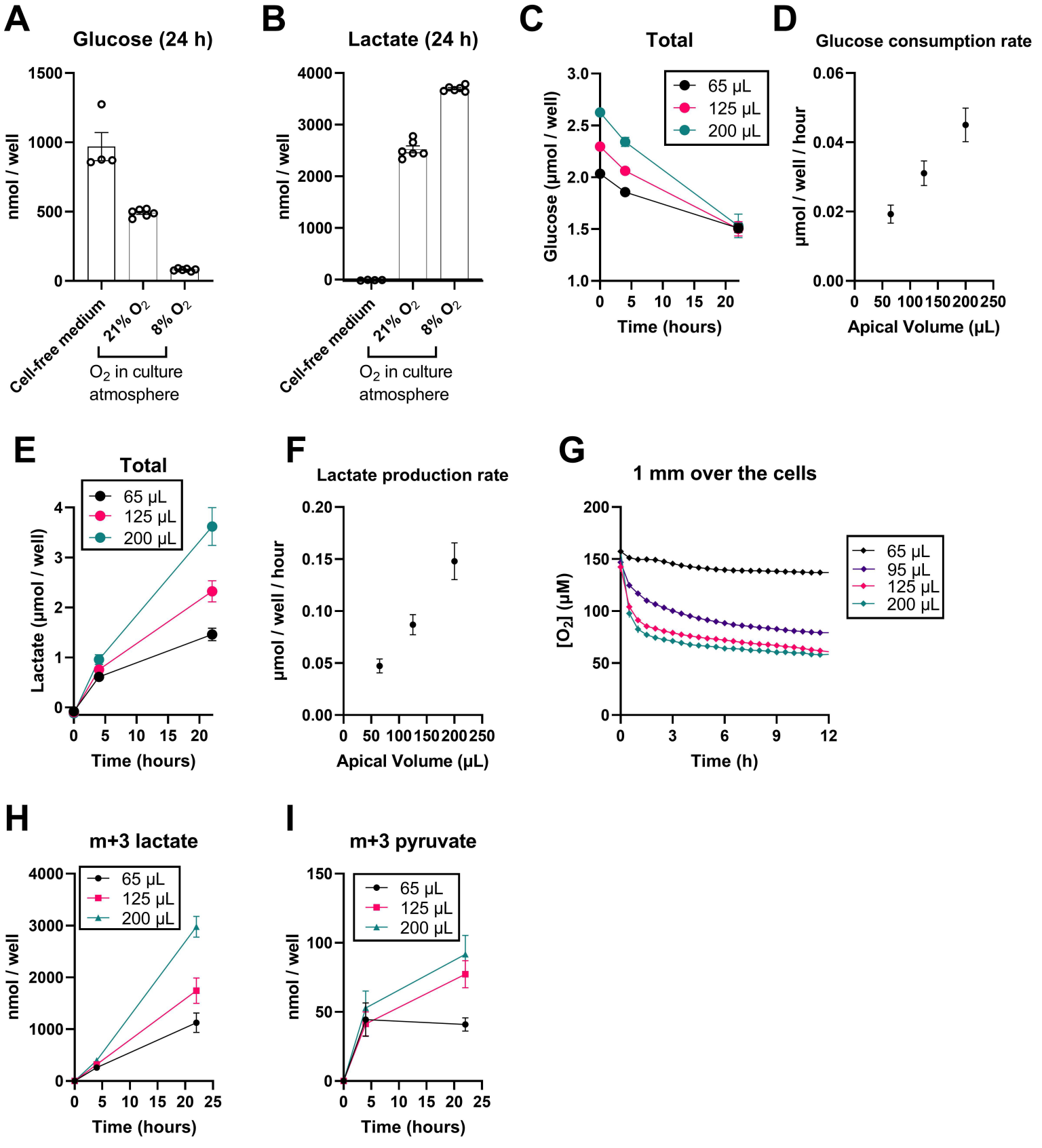
A
Glucose (24 h)
nmol / well
1500
1000
500
0
Cell-free medium
21% O2
8% O2
O2 in culture atmosphere
B
Lactate (24 h)
nmol / well
4000
3000
2000
1000
0
Cell-free medium
21% O2
8% O2
O2 in culture atmosphere
C
Total
Glucose (µmol / well)
3.0
2.5
2.0
1.5
1.0
65 µL
125 µL
200 µL
0 5 10 15 20
Time (hours)
D
Glucose consumption rate
µmol / well / hour
0.06
0.04
0.02
0.00
0 50 100 150 200 250
Apical Volume (µL)
E
Total
Lactate (µmol / well)
4
3
2
1
0
65 µL
125 µL
200 µL
0 5 10 15 20
Time (hours)
F
Lactate production rate
µmol / well / hour
0.20
0.15
0.10
0.05
0.00
0 50 100 150 200 250
Apical Volume (µL)
G
1 mm over the cells
[O2] (µM)
200
150
100
50
0
65 µL
95 µL
125 µL
200 µL
0 3 6 9 12
Time (h)
H
m+3 lactate
nmol / well
4000
3000
2000
1000
0
65 µL
125 µL
200 µL
0 5 10 15 20 25
Time (hours)
I
m+3 pyruvate
nmol / well
150
100
50
0
65 µL
125 µL
200 µL
0 5 10 15 20 25
Time (hours)

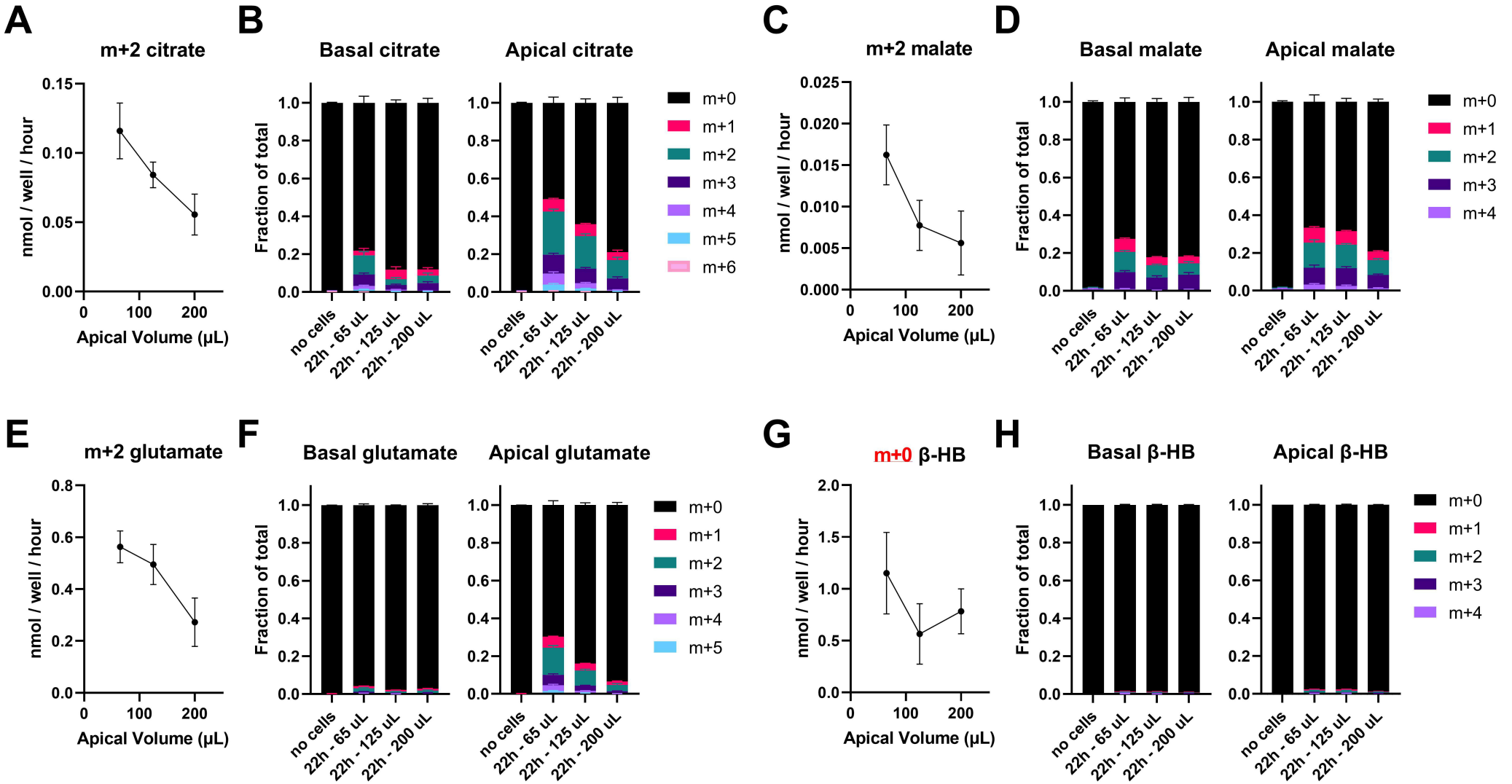
A
m+2 citrate
nmol / well / hour
Apical Volume (µL)
B
Basal citrate
Apical citrate
Fraction of total
no cells
22h - 65 uL
22h - 125 uL
22h - 200 uL
m+0
m+1
m+2
m+3
m+4
m+5
m+6
C
m+2 malate
D
Basal malate
Apical malate
E
m+2 glutamate
F
Basal glutamate
Apical glutamate
G
m+0 β-HB
H
Basal β-HB
Apical β-HB

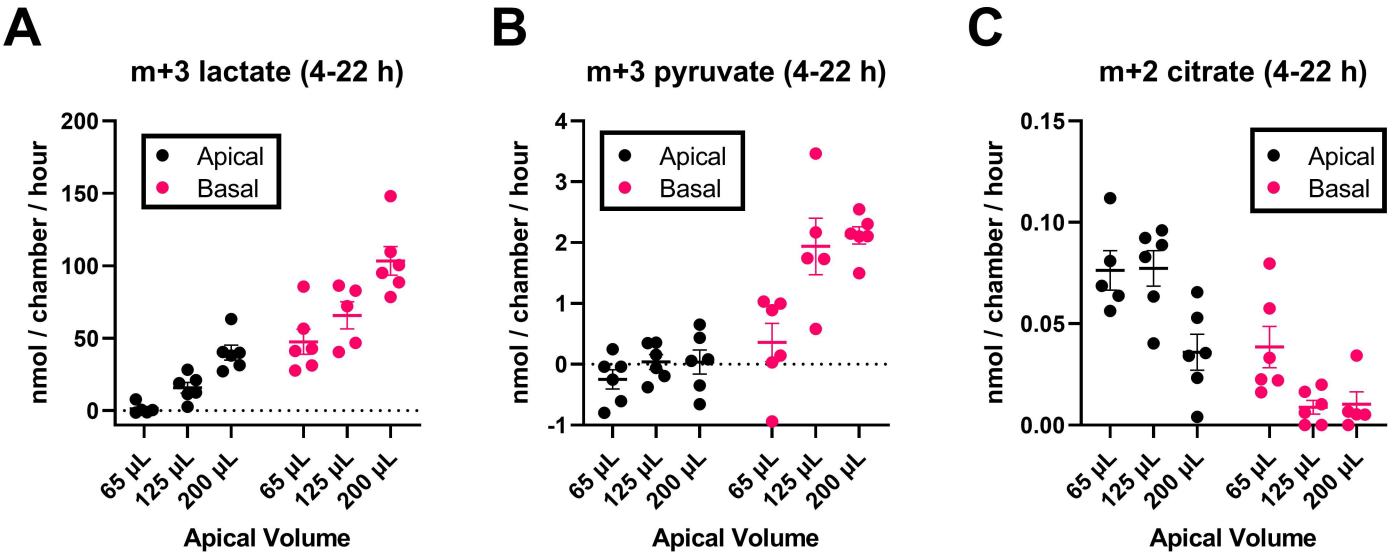
A
m+3 lactate (4-22 h)
nmol / chamber / hour
200
150
100
50
0
Apical
Basal
65 µL
125 µL
200 µL
65 µL
125 µL
200 µL
Apical Volume
B
m+3 pyruvate (4-22 h)
nmol / chamber / hour
4
3
2
1
0
-1
Apical
Basal
65 µL
125 µL
200 µL
65 µL
125 µL
200 µL
Apical Volume
C
m+2 citrate (4-22 h)
nmol / chamber / hour
0.15
0.10
0.05
0.00
Apical
Basal
65 µL
125 µL
200 µL
65 µL
125 µL
200 µL
Apical Volume

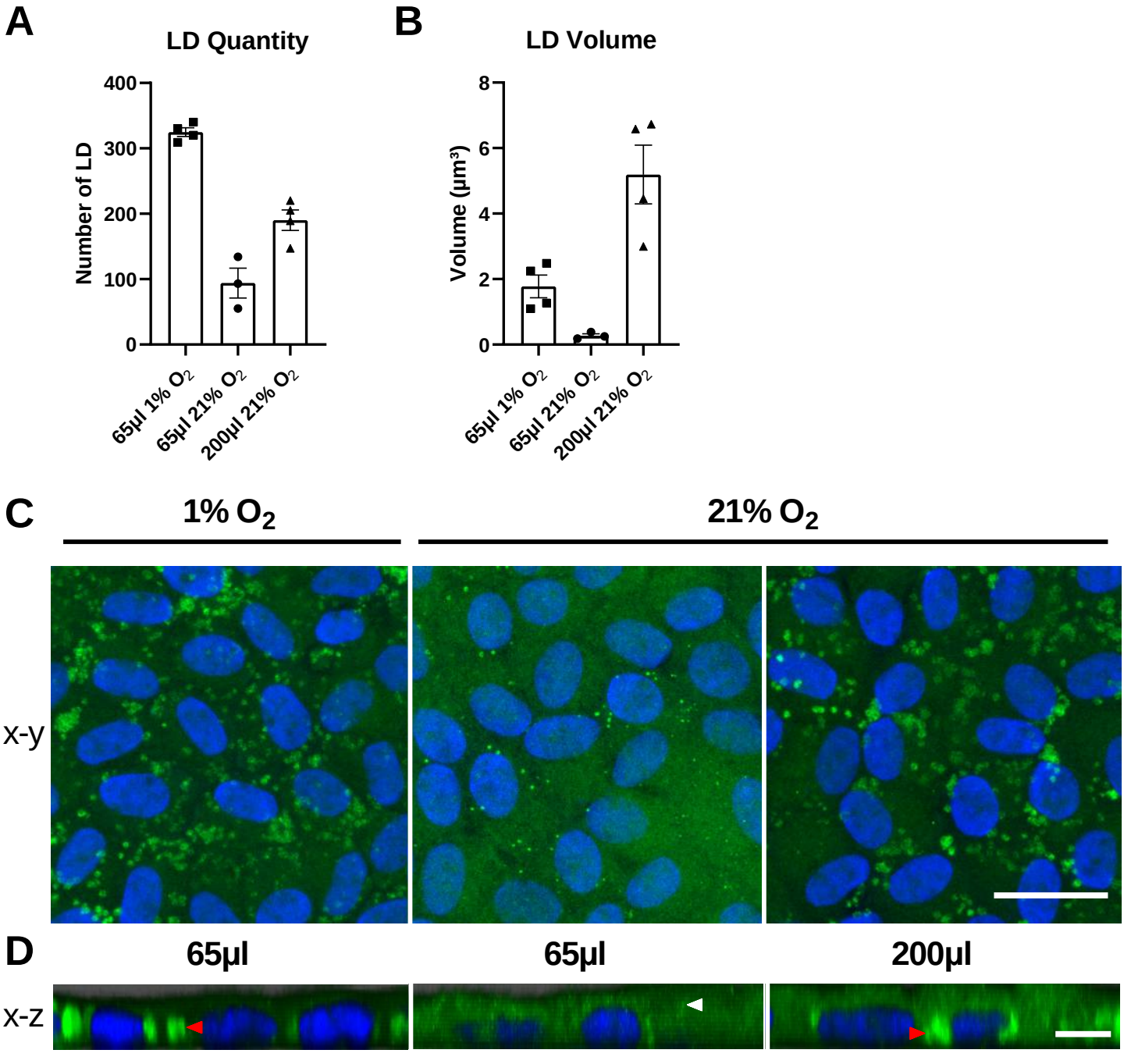
A
LD Quantity
Number of LD
400
300
200
100
0
65µl 1% O2
65µl 21% O2
200µl 21% O2
B
LD Volume
Volume (µm³)
8
6
4
2
0
65µl 1% O2
65µl 21% O2
200µl 21% O2
C
1% O2
21% O2
x-y
D
65µl
65µl
200µl
x-z